Microstructural Characterisation of Ti and V-containing Synthetic Slags Mimicking the Chemical Composition of the Slag Inclusions of Ferrous Artefacts Produced in the Iron Factory of São João de Ipanema (XIX century, Brazil)

Rafael R. Maia[a,b] , *Lucas N. Gonçalves[b], Gaspar Darin Filho[c], Augusto C. Neiva[b], Flávio Beneduce Neto[b],*

Cesar R. F. Azevedo[b] , *Fernando J. G. Landgraf[b]**

[a]Faculdade de Tecnologia de Itaquera - Professor Miguel Reale (FATEC-Itaquera), São Paulo, SP, Brasil.
[b]Universidade de São Paulo (USP), Escola Politécnica, Departamento de Engenharia Metalúrgica e de Materiais, São Paulo, SP, Brasil.
[c]Universidade de São Paulo (USP), Escola Politécnica, Departamento de Engenharia de Minhas e Petróleo, São Paulo, SP, Brasil.

In the present work, synthetic slags (FeO-SiO_2-CaO-P_2O_5-Al_2O_3-TiO_2-V_2O_5 system) mimicking the composition of the slag inclusions of Ipanema were solidified at different cooling rates. FactSage software was used to calculate the slag's phase equilibria from 500°C to 1600°C to guide the microstructural characterisation. The samples solidified with slower cooling rates featured wüstite dendrites and a eutectic-like matrix, with intradendritic (Al,V,Ti)-containing iron spinel precipitates in the wüstite. The rapidly solidified slag showed refined wüstite dendrites surrounded by a Fe-O-Si-Ca-containing amorphous single-phase matrix without intradendritic (Al,V,Ti)-containing iron spinel precipitation. The comparison of the calculated phase diagram with the as-cast microstructures showed a few discrepancies. For instance, the FactSage's database must be updated to consider the simultaneous solubility of Al, V and Ti in the thermodynamic description of the spinel phases, such as FToxid-SP-V, FToxid-SPINA, FToxid-TiSp and $(FeO)_2(TiO_2)(s)$. Finally, the intradendritic precipitation of (Al,V,Ti)-containing iron spinel phases in the wüstite of the slag inclusions indicated that an Ipanema's iron artefact was exposed to high service temperatures between 750 and 1050°C.

Keywords: *Archaeometallurgy, microstructure, synthetic slag, Iron Factory of São João de Ipanema.*

1. Introduction

The Iron Factory of São João de Ipanema had the only continuously operated blast furnaces during the XIX century in Brazil and, likely, in Latin America. The site attracted the interest of the Portuguese Crown in 1596 due to its magnetitic iron ore[1], later known to have small amounts of titanium and vanadium[2]. The twin blast furnaces were built in 1817 and operated intermittently[3] until 1919. The Brazilian Army was responsible for the Ipanema factory for most of its existence, leaving copious reports now kept in national and state Archives. The blast furnaces are still standing (Figure 1), protected as a National Heritage Site since 1964 and declared by the American Society for Metals a historic landmark[4] in 1988. Besides producing parts for the Brazilian Arsenals, cast or forged, sugarcane mill parts were the leading product in the first half of the century, and railroad maintenance parts were predominant in the second half. Samples of cast parts and forged bars produced in that plant have been kept in Museum collections, allowing for

examining its microstructure. The slag inclusions left inside the microstructure of forged bars made from the early days of the Iron Age until molten steel refining techniques in the mid-XIX century have been investigated by a large corpus of literature[5-8].

In 2016, Mamani-Calcina et al.[9] analysed forged bars produced by the Iron Factory of São João de Ipanema in 1886. EDX (Energy Dispersive X-ray Analysis) microanalyses were used to investigate the slag inclusions in the microstructure of ferrous artefacts. They observed the solid solution of vanadium (up to 3.0 at%) and titanium (up to 1.0 at%) in the wüstite dendrites of the slag inclusions. In 1980, Gleitzer[10] studied the solubility of 17 elements, including titanium, in the wüstite. The results indicate that tetravalent titanium has a solubility of 7.5% in the wüstite at 1000°C. Other works[11-13] reported the existence of a $Fe_{1-x}Ti_{0.5x}O$ wüstite. According to the phase diagram assessment by Jantzen et al.[14], the solubility of TiO_2 in the wüstite of the FeO_x-TiO_2 system increases with increasing temperature, reaching a maximum value of approximately 3 mol.% near the eutectic temperature, liquid slag → FeO

Figure 1. Twin blast furnaces, built in 1818, of the Iron Factory of São João de Ipanema. A vault was carved between the two furnaces in 1866. The upper part of the blast furnace on the right was altered in 1918. Image credited to Edgar Gomes (2006).

(cubic) + 2FeO.TiO$_2$ (cubic). Eriksson et al.[15] studied the phase equilibria in the Fe-Ti-O system using experiments and thermodynamic evaluation, in which they considered that TiO$_2$ forms a Henrian solution in the wüstite phase. Finally, Itaya et al.[16] investigated the FeO-TiO$_2$-SiO$_2$- 5%Al$_2$O$_3$ phase diagram for archaeometallurgical purposes. They observed the presence of TiO$_2$ solid solution in the dendrites of wüstite ranging from 2.4 to 6.4%. However, one work[17] mentioned that Ti is not soluble in the wüstite phase.

Many papers[5-7,9] on archaeometallurgy examined the slag inclusions of ferrous artefacts and noticed the presence of wüstite dendrites. However, none reported interdendritic precipitation in the wüstite phase of the slag inclusions until the recent work of Gonçalves[18], who performed the microstructural characterisation of the slag inclusions of an iron sample – taken from one of the reinforcing bars that crisscrossed the blast furnace of The Iron Factory of São João de Ipanema – and showed intradendritic (Al,V,Ti)-containing iron spinel precipitates in the wüstite dendrites. Previous studies[19,20] of archaeological slags also indicated the presence of intradendritic precipitates in the wüstite. Killick and Miller[19] studied the bloomery iron smelting technologies in northeastern South Africa. They analysed archaeological slag samples and showed the intradendritic precipitation of titaniferous magnetite in the wüstite dendrites. Photos[20] studied the early extractive metallurgy in north Greece. She analysed archaeological slag samples and showed the intradendritic precipitation in the wüstite dendrites. She also indicated that iron slags from various locations in Greece featured TiO$_2$ solution in the wüstite phase (from 0.34 to 10.9%).

The present work produced three synthetic slags mimicking the chemical composition of the non-metallic inclusions of Ipanema's ferrous artefacts. These slag samples were solidified at different cooling rates, and their microstructures were investigated. Additionally, the phase equilibria calculated by FactSage were used carefully to guide the microstructural characterisation of the as-cast samples (non-equilibrium state). The main objective of the present work is to reproduce the conditions for the intradendritic (Al,V,Ti)-containing iron spinel precipitation in the wüstite phase and check how this precipitation can identify the service thermal exposure range of an iron artefact (structural iron bar of a blast furnace) produced in the Iron Factory of São João de Ipanema.

2. Materials and Methodology

Three synthetic slags (CHC 195, CHC 198 and CHC 199) were prepared in a resistance furnace to mimic the average chemical composition of the slag inclusions of Ipanema's iron bar samples of the Museu Nacional Collection[9]. Metallic iron, hematite, V$_2$O$_5$, TiO$_2$, Al$_2$O$_3$, SiO$_2$, Ca$_3$P$_2$O$_8$ and CaO powders were mixed in iron crucibles. The iron crucibles were placed in a resistance furnace heated at 1400ºC under a nitrogen atmosphere and kept there for 2 hours. The temperatures were measured and controlled through a calibrated type S thermocouple. The molten slag samples were solidified at three cooling rates (furnace-cooled, air-cooled and rapidly cooled). For the furnace-cooled slag, the iron crucible containing the slag was kept in the furnace until it cooled to room temperature. For the air-cooled slag, the crucible was removed from the furnace after two hours at 1400°C and cooled outside the furnace. For the rapidly cooled slag, the crucible was removed from the furnace after 2h and poured onto an iron plate. See the chemical composition of the samples in Table 1.

2.1. Microstructural characterisation

The slag samples were prepared according to standard metallographic practices without the chemical etching[5-9].

The polished samples were characterised using optical microscopy, scanning electron microscopy (SEM), electron backscatter diffraction (EBSD) and energy dispersive spectroscopy (EDX) microanalysis. Image-J software evaluated the secondary dendrite arm spacing (SDAS) and volume fraction of the phases in the as-cast samples using backscattered electrons images (BEI). Chen et al.[21] investigated the EDX detection limits for quantifying common major and minor elements in minerals/rocks using economical desktop scanning electron microscopy/silicon drift detector energy-dispersive spectrometer. For instance, they found that the EDX microanalysis can show a detection limit close to 0.1 wt% for Al, Si and Ti. EDX microanalyses were carried out at:

- 20 kV accelerating voltage, 180 seconds acquisition time, 100x magnification, area mode, standardless method and ZAF correction to determine the bulk chemical analysis of the as-cast slag samples – each average value used at least 3 measurements.
- 15 kV accelerating voltage, 60 seconds acquisition time, point mode, standardless method and ZAF correction to determine the chemical analysis of the microconstituents – each average value used at least 4 measurements.

Finally, X-ray diffraction (XRD) was used to analyse all the slag samples (room temperature, copper K-α radiation,

45 kV, 40 mA, step mode, 0.02º step and counting time per step of 999.9 s).

2.2. Computational thermodynamics

The computational thermodynamics FactSage software was used to predict the evolution of the equilibrium phases for the synthetic slag. For this purpose, the databases FactPS (for pure substances), FSstel (for steel/ferrous systems) and FToxid (for oxide systems for slags, glasses, ceramics, and refractories) were used. The description of the modelling principles and the restrictions of the models are available on the FactSage website database documentation[22]. The most crucial data of this study were the models used to describe the molten slag phase and the solid oxide or metallic solutions (FToxid and FSstel). The Modified Quasichemical Model (MQM) describes the molten slag (liquid phase). Models based on the Compound Energy Formalism using various sublattices describe the solid phases (oxide and metal). FactSage was used to calculate the solidification sequence under equilibria conditions of the synthetic slag (FeO-SiO$_2$-CaO-P$_2$O$_5$-Al$_2$O$_3$-TiO$_2$-V$_2$O$_5$ system) at temperatures from 500ºC to 1600°C, see FactSage phases and descriptions in Table 2. Due to kinetic reasons, the number and type of phases in the phase diagram (equilibrium state) might differ from the as-cast conditions (non-equilibrium state).

Table 1. Chemical composition of synthetic slags (at%) via EDX microanalysis; balance is oxygen.

Sample	Identification	Fe	Si	Ca	P	Al	V	Ti
CHC 199	Furnace-cooled slag	27.5±1.0	6.8±0.6	4.1±0,2	2.4±0.1	2.7±0.4	0.7±0.1	0.3±0.1
CHC 195	Air-cooled slag	29.6±2.3	5.5±0.5	5.3±0.7	3.2±0.4	0.9±0.1	1.3±0.2	0.4±0.1
CHC 198	Rapidly cooled slag	28.5±3.5	8.1±1.3	4.6±0.5	2.2±0.5	2.8±0.6	0.6±0.1	0.3±0.1

Table 2. List of phases selected from FactSage databases[22] and how they were organised for the simplified phase diagram.

Fact-Sage denomination	Label in the graphs	Qualitative phase description
FSstel-BCC	Fe	BCC Fe, solid solution
FToxid-SLAGA	liquid	Molten slag, liquid oxide with solubility for Fe, Ti, V, Si, Al, Mg, Ca and other elements
FToxid-MeO_A	wustite	Fe(II)O, CaO, MgO, SrO, BaO, Mn(II)O, NiO, CoO at all compositions + Al, Fe(III), Cr(III), Li, Na, Ti(IV), Zn and Zr in dilute amounts). Wüstite (Fe$_x$O) solid solution without Si and V solubility
FToxid-SPINA	SP-V/SPINA	(Fe,Al)$_3$O$_4$ solid solution, AB$_2$O$_4$-type spinel containing Al-Co-Cr-Fe-Mg-Ni-Zn-O, cubic, solution without Si, V and Ti solubility
FToxid-SP-V		(Fe,Mg,Al,V)[Fe,Mg,Al,V,]$_2$O$_4$, vanadium spinel, cubic, solid solution without Si and Ti solubility.
FToxid-TiSp	Ti-spinels	(Mg,Fe,Mn)[Mg,Fe,Mn,Ti,Al]$_2$O$_4$, titania spinel, cubic, solution without Si and V solubility.
(FeO)2(TiO2)(s)		(FeO)$_2$(TiO$_2$), ulvöspinel, stoichiometric compound.
FToxid-OlivA	olivine	(Mg,Ca,Fe,Mn,Co,Ni,Zn)$_2$SiO$_4$ solution (olivine with high Fe and low Mg can be referred to as fayalite)
FToxid-C2SP	Ca-phosphates	Ca$_2$SiO$_4$ – Ca$_3$P$_2$O$_8$ solid solution, monoclinic
Ca3P2O8(s)		Rhombohedral Ca$_3$P$_2$O$_8$, stoichiometric
Ca3P2O8(s2)		Monoclinic Ca$_3$P$_2$O$_8$, stoichiometric

3. Results and Discussion

3.1. Phase equilibria

The phase equilibria evolution calculated by FactSage for a slag composition of 27Fe57O7Si4Ca3Al2P0.7V0.3Ti (in at%) is presented in Figure 2. For easier visualisation in this phase diagram:

- $Ca_3P_2O_8(s)$, $Ca_3P_2O_8(s2)$ and FToxid-C_2SP phases were consolidated into a single curve, labelled "Ca-phosphates", see Table 2.
- FToxid-TiSp and $(FeO)_2(TiO_2)$ phases, two Ti-containing spinels, were consolidated into a curve labelled "Ti-spinels", see Table 2.
- FToxid-SPINA (Al-containing spinel) and FToxid-SP-V (V-containing spinel) phases were consolidated into a single SP-V/ SPINA curve, see Table 2.

In Figure 2, solidification starts at 1467°C with the formation of calcium phosphate crystals, followed by the formation of wüstite at 1235°C. At 1193°C, the formation of SP-V/SPINA starts. At around 1120°C, the curves suggest the existence of a eutectic reaction, liquid → olivine + SP-V/ SPINA + Ca phosphate. Wüstite volume fraction decreases as temperatures decreases below 1000°C, corresponding to an increase in the volume fraction of the spinel phases (SP-V/SPINA and Ti-spinels). At about 640°C, the diagram suggests the existence of a eutectoid reaction in which wüstite is consumed, forming SP-V/SPINA and Fe.

In Figure 2, solidification starts at 1467°C, but the experimental melting temperature is below 1400ºC, indicating that this diagram should be used with care. Table 2 shows FactSage database limitations regarding simultaneous solid solutions for key phases, such as wüstite and iron spinels.

3.2. Furnace-cooled slag microstructure

The furnace-cooled slag microstructure is shown in Figures 3a to 3c. The estimated secondary dendrite arm spacing (SDAS) is 22 μm. Five different phases were identified in the microstructure: wüstite, calcium phosphate (Ca-phosphate), olivine and two "unknown" phases, identified as S1 and S2. Their average compositions are presented in Table 3. The primary Ca-phosphate plates and wüstite dendrites, phases which were indicated in Figure 2, are observed in the as-cast microstructure, see Figure 3a. Figure 3b shows a eutectic-like matrix containing three phases: olivine matrix (medium grey), thin Ca-phosphate plates (dark grey) and S1 plates (light grey), which is in agreement with the thermodynamic calculation – Figure 2, which foresaw a eutectic reaction, liquid → olivine + Ca-phosphate + vanadium/aluminium spinel (SP-V/SPINA) around 1100ºC. The main difference in the eutectic reaction between the as-cast sample and the calculated phase diagram is the presence of the S1 plates instead of the SP-V/SPINA phase. Electron backscatter diffraction (EBSD), see Figures 4a and 4b, confirmed the cubic crystal structure of the S2 phase, using data from wüstite (hexoctahedral) and magnetite (cubic) in the EBSD database (magnetite is an iron spinel).
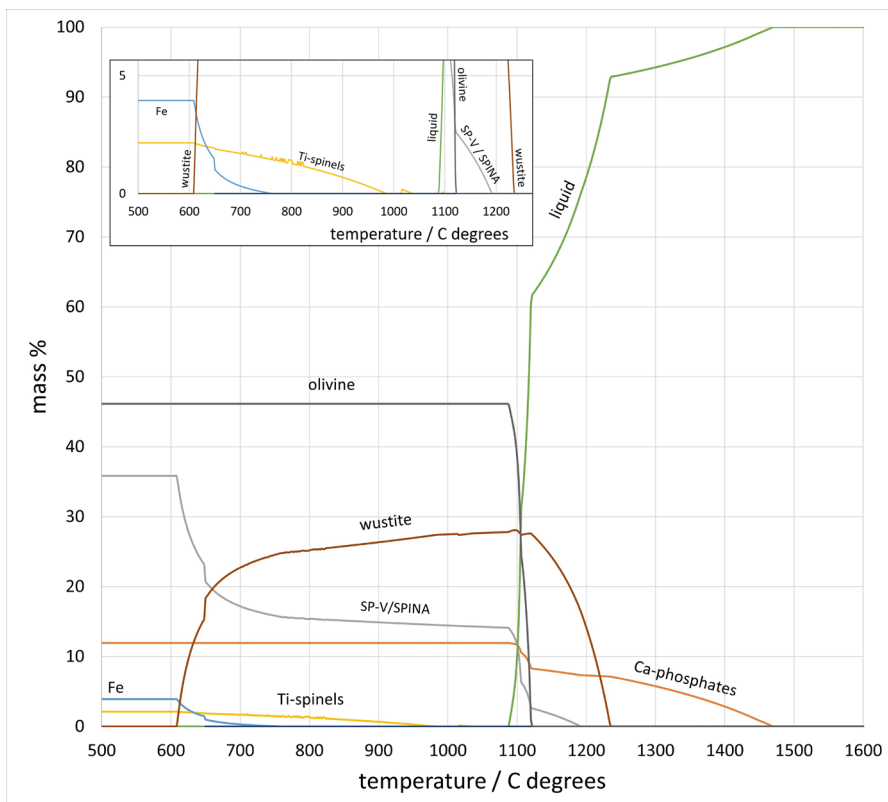

Figure 2. Phase equilibria of the furnace-cooled synthetic slag, CHC 199 sample, FactSage.

Microstructural Characterisation of Ti and V-containing Synthetic Slags Mimicking the Chemical Composition of
the Slag Inclusions of Ferrous Artefacts Produced in the Iron Factory of São João de Ipanema (XIX century, Brazil)
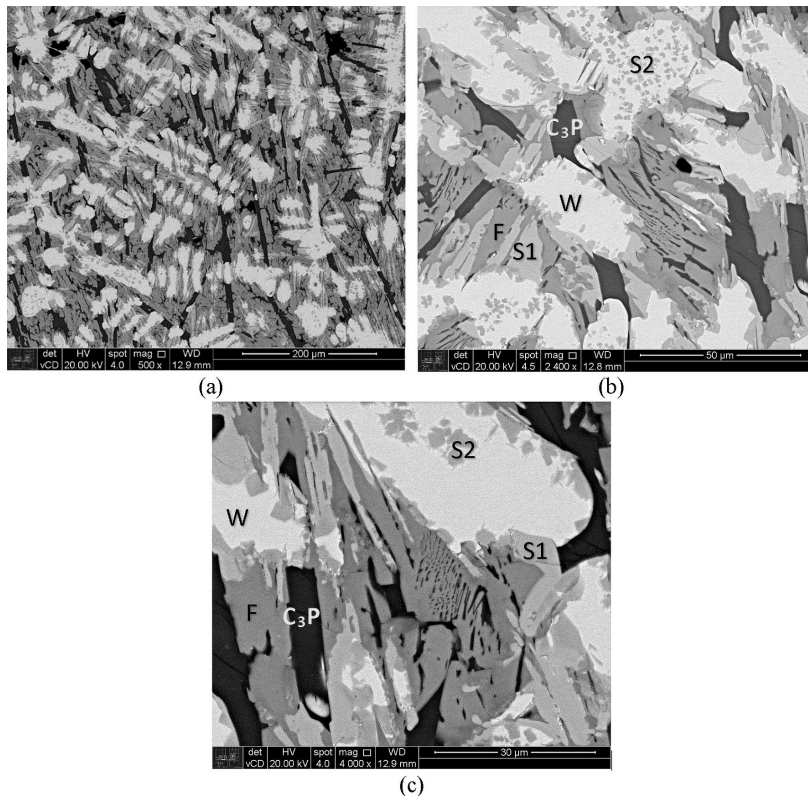
5

(a)

(b)

(c)

Figure 3. Microstructural characterisation of the furnace-cooled synthetic slag, CHC 199 sample. (a) General view of the as-cast microstructure showing wüstite dendrites (W, light grey) and the primary plates of Ca-phosphate phase (C₃P, dark grey); (b) Detail of the triplex eutectic-like matrix containing olivine/fayalite (F), Ca-phosphate thin plates (dark grey) and S1 phase (light grey). Intergranular and intradendritic precipitation of the S2 phase is observed; (c) Detail showing the formation of the S2 phase at the S1 phase/wüstite interface. SEM-BEI. See the EDX results of the five phases in Table 3.
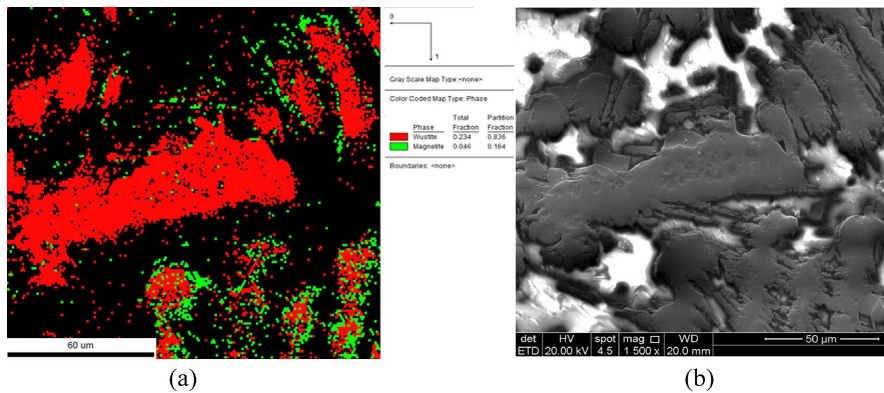

(a)

(b)

Figure 4. Discrimination of the wüstite and "magnetite", S2 phase, areas of the furnace-cooled slag sample (CHC 199 sample). (a) Green dots are regions identified that the S2 phase is cubic magnetite, and red areas are hexoctahedral wüstite, SEM-EBSD. (b) Same area, SEM-SEI.

Table 3. Chemical composition (at%) of the phases from the furnace-cooled slag obtained via EDX microanalysis, CHC 199 sample.

Phase	O	Al	Si	P	Ca	Ti	V	Fe
Wüstite	51.4±0.2	0.4±0.1	0.4±0.1	0.3±0.1	0.4±0.1	0.4±0.1	0.8±0.2	44.7±0.2
S1	50.3±0.5	3.0±0.8	5.5±0.5	0.2±0.1	0.7±0.2	0.6±0.1	1.1±0.2	38.7±1.2
S2	56.0±0.1	6.3±1.1	0.3±0.1	0.2±0.1	0.3±0.1	1.5±0.1	4.4±0.2	30.0±2.2
Olivine	54.9±0.3	0.4±0.1	14.9±1.4	0.7±0.1	1.4±0.1	0.3±0.1	0.4±0.1	25.9±2.5
Ca-phosphate	59.0±1.0	-	0.2±0.1	16.3±1.4	17.4±1.8	0.2±0.1	0.4±0.1	6.0±0.3

Figures 3b and 3c reveal the intradendritic precipitation of the S2 phase inside the wüstite. This V,Ti-containing spinel precipitate, S2 phase (Table 3), is related to the partial consumption of wüstite below 1000°C, represented in the calculated diagram by the precipitation of the Ti-spinels and SP-V/SPINA spinel phases (Figure 2). The microstructure showed no evidence of eutectoid-like decomposition of the wüstite (wustite → SP-V/SPINA + Fe), predicted in the calculated phase diagram (Figure 2).

Quantitative metallography of the as-cast sample (Figures 3a to 3c) indicated that the volume fraction of wüstite dendrites is 36%, calcium phosphate is 11%, and olivine (fayalite) is 37%. In comparison, the thermodynamic FactSage calculation indicated at 700°C a volume fraction of wüstite around 24%, calcium phosphate around 12% and olivine (fayalite) around 45%. Assuming the calculated phase diagram is reliable, the as-cast condition presents more wüstite (+50%) and less olivine (-20%) than the equilibria values, so long isothermal heat treatments of the slag sample should be used to explain the sources for these discrepancies.

Table 3 shows the average composition of the phases determined by EDX microanalysis. The chemical compositions of the S1 and S2 spinel phases differ, especially in the atomic proportion of oxygen, which is higher in the S2 phase (56 versus 50 at%). Both phases contain Al, Ti and V solid solutions, but the S1 phase is richer in Si, while the S2 phase shows a higher proportion of these solutes (~ 12.5at% versus 10.2at% in the S1 phase). The S2 phase is a $(Fe,Al,V,Ti)_3O_4$ spinel, while the S1 phase might be the iscorite (Fe_7SiO_{10} or $Fe^{2+}_5Fe^{3+}_2SiO_{10}$). This phase was identified in 1969 by Smuts et al.[23] and later recognized in several archaeological slag samples as a phase intergrown with fayalite and wüstite[24,25]. This phase, however, is not listed in the FacSage database[22].

Table 4 presents the FactSage-calculated chemical composition of the three non-stoichiometric spinel phases and the non-stoichiometric olivine, averaged along their stability range down to 500°C, and, for comparison, the composition of stoichiometric titanium spinel $(FeO)_2(TiO_2)$.

FactSage database includes the $(Fe,Al,Ti)_3O_4$ spinel, the stoichiometric $(FeO)_2(TiO_2)$ spinel, the $(Fe,Al,V)_3O_4$ spinel, and $(Fe,Al)_3O_4$ phases (see Table 2), which are simpler solid solution descriptions of more complex iron spinel phases containing simultaneous (Al,V,Ti) solid solution. Experimental phase equilibrium data must be produced to reassess the $FeO-SiO_2-CaO-P_2O_5-Al_2O_3-TiO_2-V_2O_5$ phase diagram using updated thermodynamic descriptions of the iron spinel and wüstite phases.

Figures 5a to 5c show the X-ray diffraction results of the three slag samples. Figure 5a reveals the results of the furnace-cooled slag sample, confirming the presence of four phases: wüstite, olivine/fayalite, calcium phosphate and a cubic phase associated with magnetite-like spinel, which is the $(Fe,Al,V,Ti)_3O_4$ spinel. A single extra peak could be associated with the S1 phase but did not fit any iscorite peaks ($FeO-Fe_2O_3-SiO_2$ system XRD data).
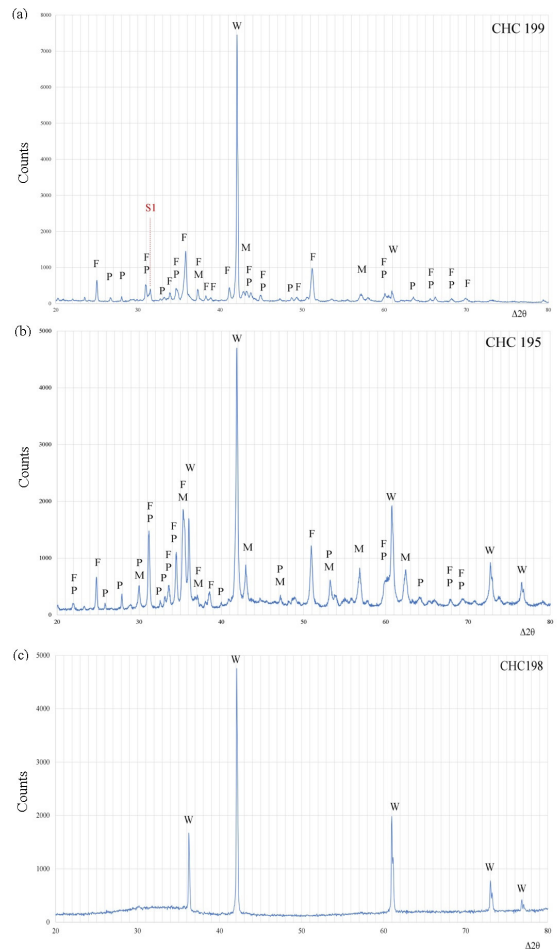

Figure 5. XRD of the as-cast samples. (a) Furnace-cooled as-cast slag (CHC 199 sample); (b) Air-cooled as-cast slag (CHC 195 sample); (c) Rapidly cooled as-cast slag (CHC 198 sample) showing an amorphous matrix. W is wüstite, F is fayalite, P is $Ca_3P_2O_8$, and M is a magnetite-like spinel.

Table 4. Composition (at%) of stoichiometric $(FeO)_2(TiO_2)$ and non-stoichiometric olivine and spinel phases, averaged along their range of existence down to 500°C, using FactSage, CHC 199 chemical composition.

Phase	O	Al	Si	Ca	Ti	V	Fe
FToxid-OlivA	57.1	-	14.3	1.0	-	-	27.6
FToxid-SP-V	57.1	13.9	-	-	-	3.6	25.3
FToxid-SPINA	57.1	25.4	-	-	-	-	17.5
FToxid-TiSp	57.1	2.3	-	-	15.3	-	25.3
$(FeO)_2(TiO_2)$	57.1	-	-	-	14.3	-	28.6

3.2. Air-cooled slag microstructure

Figures 6a to 6c show the microstructure of the CHC 195 sample. Wüstite dendrites containing intergranular and intradendritic precipitation are observed in a duplex eutectic-like matrix formed by Ca-phosphate (black plates) and olivine (grey matrix). Quantitative metallography indicated that the volume fraction of wüstite dendrites is 32%, calcium phosphate is 9%, and olivine is 35%. These results are not far from the results of the CHC 199 sample (wüstite of 36%, calcium phosphate of 11%, and olivine of 37%), see Figures 3a to 3c. The estimated secondary dendrite arm spacing is 18 μm. The eutectic-like duplex matrix agrees with the eutectic reaction in the calculated phase diagram (Figure 2), but the hypothetical SP-V/ SPINA phase is not observed in the microstructure. There is a difference between the eutectic matrix microstructure of the furnace-cooled sample (see Figures 3-a to 3-c) and the air-cooled, concerning the number of phases and the morphology due to the higher cooling rate and changes in the chemical composition (Table 1).

The intradendritic and intergranular precipitates (S phase) in the wüstite dendrites (see Figure 6c) have the same composition, described as $(Fe,Al,V,Ti)_3O_4$ spinel in Table 5. This spinel features a different chemical composition from the intradendritic precipitates of the previous sample; see the S2 spinel phase in Figures 3a to 3c and Table 3. Still, they both can be treated as a $(Fe,Al,V,Ti)_3O_4$ spinel. This spinel is related to the partial consumption of wüstite below 1000°C, represented in the calculated diagram by the precipitation of Ti-spinels and SP-V/SPINA spinel phases, see Figure 2. The wüstite dendrites retained some Ti and V in solid solution after the $(Fe,Al,V,Ti)_3O_4$ spinel precipitation, see Table 5. The microstructure showed no evidence of eutectoid-like decompositions of wüstite (wustite → SP-V/ SPINA + Fe) predicted in the calculated phase diagram (Figure 2). Figure 5b shows the X-ray diffraction results of the air-cooled slag sample, confirming the presence of four phases: wüstite, olivine/fayalite, calcium phosphate and a cubic phase associated with magnetite-like spinel, which is the $(Fe,Al,V,Ti)_3O_4$ spinel.
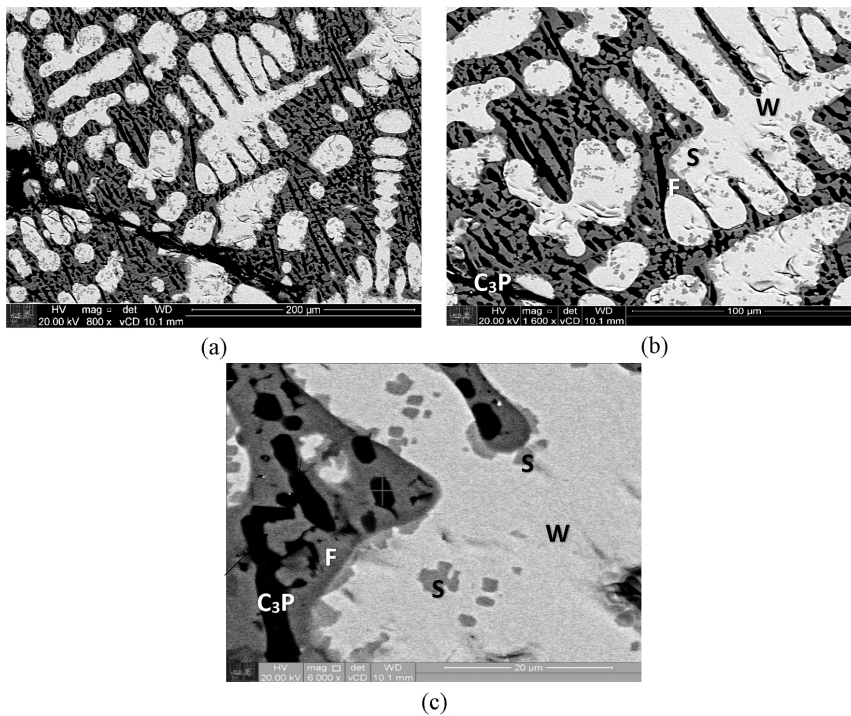

(a)

(b)

(c)

Figure 6. Microstructural characterisation, CHC 195 sample, air-cooled synthetic slag. (a) and (b) Wüstite dendrites (light grey) surrounded by a eutectic-like duplex matrix of olivine (F, grey matrix) and calcium phosphate (C_3P, black plates); (c) Detail showing the intergranular and intradendritic precipitation of a spinel phase, S, $(Fe,Al,V,Ti)_3O_4$, in the wüstite. SEM-BEI. See the EDX results of the four phases in Table 5.

Table 5. Chemical composition (at%) of phases found in air-cooled slag obtained via EDX microanalysis, CHC 195 sample.

Phase	O	Al	Si	P	Ca	Ti	V	Fe
Wüstite	50.0±0.8	-	-	-		0.6±0.1	1.9±0.1	47.5±0.2
S	57.0±2.1	3.6±0.5	0.4±0.1	-	-	5.0±1.1	10±1	24.0±1.2
Olivine	57.0±1.2	-	14.9±1.3	-	2.6±0.8	-	-	25.4±0.2
Ca-phosphate	61.0±1.9	-	1.2±0.3	14.0±1.6	19.0±1.7	-	0.6±0.1	3.1±0.3

Figure 7 presents a FactSage calculation of the Ti partition during cooling for the CHC 195 composition, indicating there is a 0.48wt%Ti-supersaturation in the wüstite, promoting the precipitation of Ti-spinels, such as FToxid-TiSp and (FeO)2(TiO2)(s) (see Table 2).

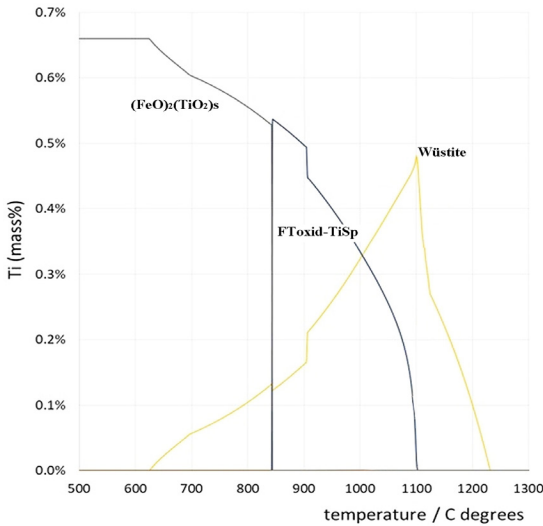**Figure 7.** Calculated Ti partition between the wüstite and Ti-spinels (FToxid-TiSp and (FeO)$_2$(TiO$_2$)(s)) in the air-cooled slag (CHC 195 sample), FactSage.

3.3. Rapidly cooled slag microstructure

The microstructure of the rapidly cooled sample (CHC 198) is shown in Figures 8a and 8b. The secondary dendrite arm spacing is 2 μm, revealing wüstite dendrites in a single-phase matrix, probably amorphous, with some idiomorphic crystals. The chemical analyses of the three phases are presented in Table 6. Wüstite contains most of the Ti and V of the slag (1.9at%V and 0.6at%Ti). Intergranular and intradendritic (Al,V,Ti)-containing iron spinel precipitates in the wüstite dendrites were not observed, resembling the "precipitationless" wüstite dendrites observed in the microstructure of the slag inclusions of iron artefacts[5-9]. The cooling rate during the processing of these iron artefacts is high enough to avoid intradendritic and intergranular precipitation of iron spinel in the wüstite dendrites. Figure 5c shows the X-ray diffraction results of the rapidly cooled slag sample, confirming the presence of wüstite and an amorphous phase. The cooling rate is much further away from the equilibria conditions than the previous samples, so the matrix is amorphous (the crystalline phase exhibits sharp distinct peaks, while the amorphous phase shows a hump in the diffractogram). The absence of Ca-phosphate in the microstructure contradicts the prediction of the FactSage software, but it is an indication that the chosen melting temperature for the experiments, 1400°C, allowed for an initial fully molten state.

3.4. Final Remarks

Many papers[5-7,9] on archaeometallurgy have examined the slag inclusions of ferrous artefacts and noticed the
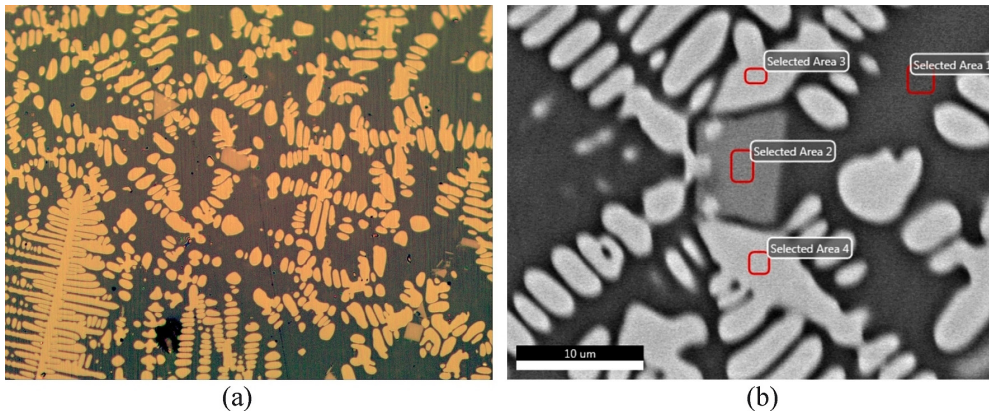

Figure 8. Microstructural characterisation, CHC 198 sample, rapidly cooled synthetic slag. (a) Wüstite dendrites, containing 0.5at%Ti and 1.5at% V in a Fe-O-Si-Ca-containing single-phase matrix, OM; (b) Detail of Fe-O-V-Al-containing idiomorphic phase, see Table 6, SEM-BEI.

Table 6. Chemical composition of phases found in rapidly cooled slag (at%), obtained via EDX microanalysis, CHC 198 chemical composition.

Phase	O	Al	Si	P	Ca	Ti	V	Fe
Wüstite	52.0±0.1	0.8±0.1	0.6±0.1	-	0.6±0.2	0.5±0.1	1.5±0.2	44.0±0.4
Matrix	59.3±0.7	3.6±0.4	11.6±1.0	3.3±0.2	6.7±0.3	0.2±0.1	-	15.2±1.7
Idiomorphs	58.6±0.7	6.5±0.5	0.2±0.1	-	0.4±0.1	1.2±0.1	8.1±0.5	24.8±1.2

Microstructural Characterisation of Ti and V-containing Synthetic Slags Mimicking the Chemical Composition of
the Slag Inclusions of Ferrous Artefacts Produced in the Iron Factory of São João de Ipanema (XIX century, Brazil)

9

presence of wüstite dendrites. However, none have reported intradendritic precipitation in the wüstite phase of the slag inclusions. Mamani-Calcina et al[9]. have shown that the slag inclusions of iron bars from Iron Factory of São João de Ipanema made in 1886 contained a small amount of Ti and V, most of it concentrated in the wüstite dendrites. Nevertheless, no Ti or V-containing precipitates were found inside the slag inclusions in the literature[5,7-9], except in the slag remnants investigated by Killick and Miller[19] and Photos[20]. The absence of precipitates in the wüstite dendrites of the slag inclusions in the ferrous artefacts analysed by Mamani-Calcina et al[9]. indicates that the cooling rate after the refining operation of these artefacts is rapid enough to avoid the precipitation of (Al,V,Ti)-containing iron spinels in the wüstite dendrites.

Depending on the thermal history of the ferrous artefact, the intradendritic precipitation of (Al,V,Ti)-containing iron spinels and the eutectoid reaction might occur in the slag inclusions. For instance, the microstructural characterisation of a XIX century iron hammer[26] "showed an unusual feature: the primary wüstite dendrites suffered partial decomposition into magnetite plates (Fe_3O_4) and ferrite halos (Fe), with the ferrite halos between the primary wüstite dendrite and the interdendritic region. The wüstite decomposition is likely related to the high service temperature at the surface of the forging hammer". The authors suggested that the high service temperature was below the eutectoid temperature (~ 560ºC). In the present work, the synthetic slags did not show the eutectoid decomposition of wüstite into metallic iron and spinel (wüstite → Fe + SP-V/SPINA).

Figures 9a to 9d show the slag inclusion microstructure of a structural iron bar – sampled from one of the Ipanema's blast furnace reinforcing bars exposed in the opening of a vault between the twin furnaces. Those bars were inside the masonry of the furnace for 45 years[18]. The microstructure of the slag inclusions features wüstite dendrites (light grey) in a duplex matrix, olivine (dark grey) and Ca phosphate (black). Similar to the slow cooled slag microstructure, two phases are seen in connection to the wüstite phase. A phase (richer in Ti, Al and Si, Table 7) surrounds the wüstite dendrites, similar to the S1 phase. Intergranular and intradendritic precipitation similar to the S2 phase found in the wüstite dendrites of the slow-cooled slag sample (Figures 3a to 3c,). The microstructure showed no evidence of eutectoid-like decompositions of wüstite (wustite → SP-V/SPINA + Fe) predicted in the calculated phase diagram (Figure 2). These results suggest that this structural iron bar was exposed to high service temperatures - below the eutectic at 1120ºC but above the eutectoid temperatures at 640ºC, Figure 2.
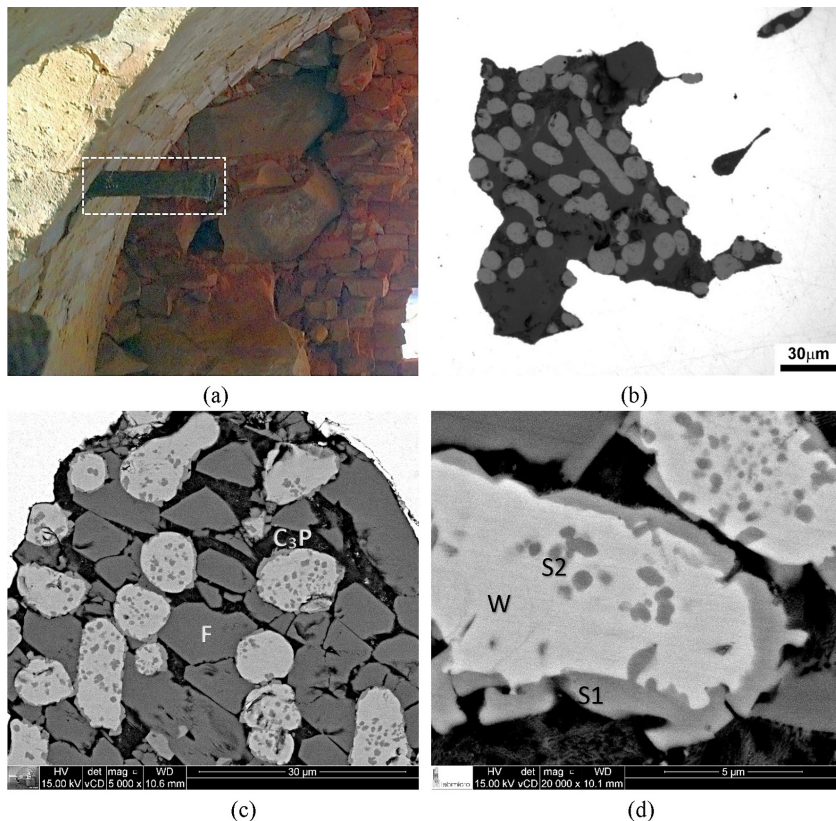

(a)

(b)

(c)

(d)

Figure 9. Microstructural characterisation of the slag inclusions in an iron bar - exposed to high temperature for decades, CHC 154 sample[18]. (a) Structural iron bar inside a blast furnace, Iron Factory of São João de Ipanema; (b) and (c) Wüstite dendrites (W, light grey) in a coarse duplex matrix containing olivine (F, dark grey) and calcium phosphate (C_3P, black) phases, OM and BEI-SEM; (d) Detail showing intradendritic (Ti,V,Al)-containing spinel precipitation (S2 phase) featuring ~ 3at%Ti, 1.5at%Al and 0.9at%V and intergranular (Si,Al,Ti,V)-containing spinel precipitation (S1 phase) featuring ~ 5.7%Ti, 4.2at% Al, 2.2at% Si, 0.8at% V, see Table 7. SEM-BEI.

Table 7. Chemical composition (at%) of the precipitates in the wüstite dendrites, slag inclusions of the blast furnace structural iron bar obtained via EDX microanalysis, CHC 154 sample[18].

Phase	O	Al	Si	Ca	Ti	V	Fe
Wüstite	48.6±0.5	0.4±0.1	0.4±0.1	0.1±0.1	1.0±0.6	0.4±0.1	47.2±1.0
S1	53.8±2.0	4.2±1.3	2.2±1.1	1.1±0.5	5.7±1.3	0.8±0.2	30.2±3.9
S2	48.2±0.9	1.5±0.6	0.3±0.2	0.3±0.1	3.0±0.4	0.9±0.1	44.1±2.2
Olivine	55.7±0.9	0.4±0.2	13.8±0.4	1.4±0.5	0.2±0.1	0.2±0.1	25.8±0.9

The chemical compositions of the S1 and S2 phases differ, especially in the atomic proportion of oxygen, which is higher in the S1 phase (54 versus 48 at%). Additionally, both phases contain Si, Al, Ti and V solid solutions, but the S1 phase shows a higher proportion of these solutes (~ 12.9at% versus 5.7at% in the S2 phase). These EDX results differ from the CHC 199 sample (see Table 3), but the S1 phase is much richer in Si for both samples.

The results of the present work confirm that the microstructure of the slag and slag inclusion can reveal the thermal history of the ferrous artefacts.

- The eutectic reaction was suppressed during the as-cast slag sample cooled at the fastest rate, promoting the formation of an amorphous matrix.
- The intradendritic precipitation of iron spinel in the wüstite dendrites did not occur in the as-cast slag sample colled at the highest cooling rate;
- The eutectoid decomposition of the wüstite was not observed in any of the as-cast slag samples.

It is interesting to consider that a ferrous artefact presents slag inclusion of different sizes, chemical compositions and origins (furnace refractory, ore, raw materials, processing slag), so the study of the slag inclusion microstructure to identify the provenance of a ferrous artefact or each one of its non-metallic inclusions is a fascinating field to understand the history of steelmaking in Brazil.

4. Conclusions

1. Furnace-cooled slag showed primary calcium phosphate plates and wüstite dendrites containing intergranular and intradendritic precipitation of a $(Fe,Al,V,Ti)_3O_4$ spinel phase (S2), as predicted in the calculated phase diagram. The eutectic-like matrix, indicated by the calculated phase diagram, contained a (Fe,Si,Al,V,Ti)-containing phase (S1), calcium phosphate and olivine phases.

2. Air-cooled slag showed wüstite dendrites containing intergranular and intradendritic precipitation of a $(Fe,Al,V,Ti)_3O_4$ spinel phase (S) immersed in a eutectic-like duplex matrix containing calcium phosphate and olivine.

3. Rapidly cooled slag showed refined wüstite dendrites without intergranular and intradendritic precipitation of iron spinel phase and surrounded by an amorphous matrix containing Fe, Si, P, Al, and Ca. A small amount of primary idiomorphic (V,Al,Ti)-containing iron spinel was observed.

4. The precipitation of (Al,V,Ti)-containing iron spinel in the wüstite phase of the slag samples depended on the cooling rate (thermal history), as this precipitation did not occur in the rapidly solidified sample.

5. The eutectoid decomposition of wüstite into metallic iron and spinel, predicted in the calculated phase diagram, was not observed in any of the slag samples.

6. The FactSage phase diagram helped the understanding of the as-cast microstructures of air-colled and furnace-cooled synthetic slags. Still, its database must be optimised to consider the simultaneous solubility of Al, Si, V and Ti in the spinel and other phases, such as FToxid-SP-V, FToxid-SPINA, FToxid-TiSp and (FeO)2(TiO2)(s). These phases are simpler thermodynamic descriptions of complex iron spinel and other phases containing simultaneous (Al,Si,V,Ti,P,Ca) solid solution. Additionally, the thermodynamic description of the wüstite phase, FToxid-MeO_A, does not consider the solubility of Si, P and V.

7. The precipitation of (Al,V,Ti)-containing iron spinel phases in the wüstite of the slag inclusions indicated that the structural iron bar of the Iron Factory of São João de Ipanema´s blast furnace was exposed to service temperatures between 750 and 1050ºC.

5. Acknowledgments

6. References

1. Rogers EJ. The iron and steel industry in colonial and imperial Brazil. Americas. 1962;19(2):172-84.

2. Guarino V, Azzone RG, Brotzu P, Gomes CB, Melluso L, Morbidelli L, et al. Magmatism and fenitization in the Cretaceous potassium-alkaline-carbonatitic complex of Ipanema São Paulo State, Brazil. Mineral Petrol. 2012;104(1-2):43-61.

3. Landgraf FJG, Araújo PEM, Schroeder R. Ipanema und die Deutschen. In: Kupfer EE, Bolle W, editors. Martius-Staden-Jahrbuch. São Leopoldo: Oikos; 2016, p. 149-63.

4. ASM International. ASM historical landmarks [Internet]. 2023 [cited 2023 May 16]. Available from: https://www.asminternational.org/membership/awards/historical-landmarks

5. Buchwald VF, Wivel H. Slag analysis as a method for the characterization and provenancing of ancient iron objects. Mater Charact. 1998;40(2):73-96.

6. Charlton MF, Blakelock E, Martinón-Torres M, Young T. Investigating the production provenance of iron artifacts with multivariate methods. J Archaeol Sci. 2012;39(7):2280-93.

7. Dillmann P, L'Héritier M. Slag inclusion analyses for studying ferrous alloys employed in French medieval buildings: supply of materials and diffusion of smelting processes. J Archaeol Sci. 2007;34(11):1810-23.

8. Gordon R. Process deduced from ironmaking wastes and artefacts. J Archaeol Sci. 1997;24(1):9-18.

9. Mamani-Calcina EA, Landgraf FJG, Azevedo CRF. Investigating the provenance of iron artifacts of the Royal Iron Factory of São João de Ipanema by hierarchical cluster analysis of EDS microanalyses of slag inclusions. Mater Res. 2016;20(1):119-29.

10. Gleitzer C. Diversity and complexity of the wustite solid solutions I-tentative rationalization of the miscibility data and classification of the wustite ternary fields and of the postsaturation reactions. Mater Res Bull. 1980;15(4):507-19. http://dx.doi.org/10.1016/0025-5408(80)90058-6.

11. Geva S, Farren M, John DHS, Hayes PC. The effects of impurity elements on the reduction of wustite and magnetite to iron in CO/CO_2 and H_2/H_2O gas mixtures. Metall Trans, B, Process Metall. 1990;21(4):743-51. http://dx.doi.org/10.1007/BF02654253.

12. Nishio-Hamane D, Yagi T, Ohshiro M, Niwa K, Okada T, Seto Y. Decomposition of perovskite $FeTiO_3$ into wüstite $Fe_{1-x}Ti_{0.5x}O$ and orthorhombic $FeTi_3O_7$ at high pressure. Phys Rev B Condens Matter Mater Phys. 2010;82(9):092103. http://dx.doi.org/10.1103/PhysRevB.82.092103.

13. Iwamoto N. Oxide inclusions formed in steels (report I): deoxidation products by Al, Si, Mn, Ti, V. Trans JWRI. 1974;3:41-51.

14. Jantzen T, Hack K, Yazhenskikh E, Müller M. Addition of TiO_2 and $Ti2O_3$ to the Al_2O_3-FeO-Fe_2O_3-MgO system. Calphad. 2018;62:187-200. http://dx.doi.org/10.1016/j.calphad.2018.05.009.

15. Eriksson G, Pelton AD, Woermann E, Ender A. Measurement and thermodynamic evaluation of phase equilibria in the Fe-Ti-O system. Ber Bunsenges Phys Chem. 1996;100(11):1839-49. http://dx.doi.org/10.1002/bbpc.19961001114.

16. Itaya H, Watanabe T, Hayashi M, Nagata K. Phase diagram of FeO-TiO_2-SiO_2-5%Al_2O_3 slag (phase diagram of smelting slag of titanium oxide bearing iron sand). ISIJ Int. 2014;54(5):1067-73. http://dx.doi.org/10.2355/isijinternational.54.1067.

17. Prabowo SW, Longbottom RJ, Monaghan BJ, del Puerto D, Ryan MJ, Bumby CW. Phase transformations during fluidized bed reduction of New Zealand titanomagnetite ironsand in hydrogen gas. Powder Technol. 2022;398:117032. http://dx.doi.org/10.1016/j.powtec.2021.117032.

18. Gonçalves LN. Arqueometalurgia: Investigação de precipitação na wustita de escórias de objetos fabricados na Fábrica de Ferro de Ipanema [thesis]. São Paulo: Universidade de São Paulo; 2021 [cited 2023 May 16]. Available from: https://bdta.abcd.usp.br/directbitstream/8c5699e9-1991-4fd3-aa39-2646f2848631/LucasNalessoGoncalves%20TF-...

19. Killick D, Miller D. Smelting of magnetite and magnetite ilmenite iron ores in the northern Lowveld, South Africa, ca. 1000 CE to ca. 1880 CE. J Archaeol Sci. 2014;43:239-55.

20. Photos E. Early extractive iron metallurgy in Greece: a unified approach to regional archaeometallurgy [thesis]. London: University of London; 1987.

21. Chen Y, Chen Y, Liu Q, Liu X. Quantifying common major and minor elements in minerals/rocks by economical desktop scanning electron microscopy/silicon drift detector energy-dispersive spectrometer (SEM/SDD-EDS). Solid Earth Sciences. 2023;8(1):49-67. http://dx.doi.org/10.1016/j.sesci.2022.12.002.

22. CRCT: Centre for Research in Computational Thermochemistry. FactSage database documentation: solutions (oxides) in FToxid [Internet]. 2023 [cited 2023 May 16]. Available from: https://www.crct.polymtl.ca/fact/documentation/FToxid/FToxid_help.htm

23. Smuts J, Steyn GD, Boeyens JCA. The crystal structure of an iron silicate, iscorite. Acta Crystallogr B. 1969;B25(7):1251-5.

24. Rose D, Endlicher G, Mucke A. The occurrence of "Iscorite" in Medieval iron slags. Journal of the Historical Metallurgy Society. 1990;24:27-32.

25. Hauptmann A. The investigation of archaeometallurgical slag. In: Roberts BW, Thornton CP, editors. Archaeometallurgy in global perspective. New York: Springer; 2014. 865 p.

26. Landgraf FJG, Ribeiro MYQ, Rosa GIL, Carvalho PSG, Rodrigues DL, Maia RR, et al. Archaeometallurgy of ferrous artefacts of the Patriótica Iron Factory (XIX century, Ouro Preto, Brazil). REM Int Eng J. 2021;74(4):483-501.